Multiplane deconvolution in underwater acoustics: Simultaneous estimations of source level and position

Maxime Polichetti, Valentin Baron, Jerome I. Mars, Barbara Nicolas

JASA EXPRESS LETTERS

Multiplane deconvolution in underwater acoustics: Simultaneous estimations of source level and position

Cite as: JASA Express Lett. 1, 076001 (2021); https://doi.org/10.1121/10.0005513
Submitted: 16 March 2021 • Accepted: 10 June 2021 • Published Online: 08 July 2021

Maxime Polichetti, Valentin Baron, Jérôme I. Mars, et al.

JASA EXPRESS LETTERS ARTICLE asa.scitation.org/journal/jel

Multiplane deconvolution in underwater acoustics: Simultaneous estimations of source level and position

Maxime Polichetti,[1] Valentin Baron,[1,a)] Jérôme I. Mars,[1] and Barbara Nicolas[2,b)]
[1]Univ. Grenoble Alpes, CNRS, Grenoble-INP, GIPSA-Lab, 38000 Grenoble, France
[2]Univ Lyon, INSA-Lyon, Université Claude Bernard Lyon 1, CNRS, Inserm, CREATIS UMR 5220, U1294, F-69100, LYON, France
valentin.baron@microdb.fr, jerome.mars@gipsa-lab.grenoble-inp.fr, barbara.nicolas@creatis.insa-lyon.fr

Abstract: In many acoustic imaging applications, conventional beamforming (CBF) cannot provide both accurate position and source level estimates simultaneously. Also, the CBF acoustic maps suffer from many artifacts due to the spreading of large point-spread-functions. An original CLEAN deconvolution procedure, including an additional plane containing out-of-plane interfering sources, is proposed here to achieve simultaneous localization, source level estimation, and de-noising. The approach is illustrated using experimental data mimicking a challenging deep-sea mining configuration: an underwater acoustic source of interest is located 700 m below the sea surface, tens of meters from a 3 m-length array, with boat noise as the disturbing source.

[Editor: Matthew A. Dzieciuch] https://doi.org/10.1121/10.0005513

Received: 16 March 2021 **Accepted:** 10 June 2021 **Published Online:** 8 July 2021

1. Introduction

Acoustic imaging generally follows a common scenario: a source of interest has to be located on an imaging plane using an acoustic array of microphones, and a strong disturbing source (possibly out-of-plane) interferes with it, deteriorating the acoustic maps and preventing characterization of the source of interest (e.g., position, level, spectrum estimation). The present study addresses acoustic imaging with an original strategy applied to the specific context of underwater deep-sea mining.

Underwater acoustic measurements monitor what happens in the ocean, which is composed of many acoustic noises: boats, submarines, whales, etc. (Kuperman and Roux, 2007). Many parameters of these acoustic sources (e.g., position, acoustic level, spectrum) are of great interest for research, defense, or industrial purposes. However, all these acoustic sources are likely to interfere with each other, hindering correct monitoring. Typically, one or several hydrophones used to monitor a source of interest near the seafloor can be easily contaminated with the noise emitted by a passing boat (Clark *et al.*, 2009; Li *et al.*, 2019; Pham *et al.*, 2019). In the case of acoustic imaging in deep-sea mining environments, surface boat noise is recorded by the acoustic array and prevents the estimation of both the position and level of the acoustic sources of interest on the seafloor, as it generates strong artifacts on acoustic maps (Pham *et al.*, 2019).

A classical acoustic imaging technique for position or level estimation is conventional beamforming (CBF) (Sarradj, 2012b). However, CBF often returns inaccurate source level estimations, as several sources overlap each other in the imaging plane because of the wide point-spread-function (PSF). These disturbing sources can be located at the same depth as the source of interest but also anywhere else in the water column. Adaptive beamforming (Capon, 1969) is a common solution for improved resolution and sidelobe rejection in many acoustic imaging fields. However, it is subject to two main limitations: its high computational cost and, mainly, its instability to steering vector mismatch (Merino-Martínez *et al.*, 2019). Many strategies to make adaptive beamforming more robust have been proposed, but most of them require a very empirical tuning of a hyperparameter (e.g., diagonal loading regulation) (Leclère *et al.*, 2017; Stoica *et al.*, 2003). High-resolution beamforming, such as MUSIC beamforming, has been proposed to enhance the localization of the source of interest, but the artifact from the out-of-plane disturbing source remains as a ghost source on the plane of interest. Furthermore, MUSIC cannot be used for source level estimations (Pham *et al.*, 2019).

To solve this issue in aeroacoustics, deconvolution post-processing approaches are commonly used (Leclère *et al.*, 2017; Merino-Martínez *et al.*, 2019). Deconvolution aims to remove the effect of PSF from CBF maps to improve both localization and source level estimation. Approaches such as deconvolution approach for the mapping of acoustic

a)Also at: MicrodB, 28 Chemin du Petit Bois, 69130 Ecully, France.
b)Author to whom correspondence should be addressed, ORCID: 0000-0001-9062-1115.

sources (DAMAS) (Brooks and Humphreys, 2006) or non-negative least squares (NNLS) (Ehrenfried and Koop, 2007) have recently been introduced for underwater acoustic imaging in shallow water environments (Sun *et al.*, 2020). These methods consist in solving an inverse problem to find the accurate source distribution (source position and level) considering a given CBF map and a set of predetermined PSFs. However, they suffer from heavy computational costs: they require a huge number of PSFs to be computed (as many as the pixel number, several hundreds or thousands) and about one hundred iterations (or more) to converge (Sun *et al.*, 2020). Faster versions of these algorithms require assumptions for shift invariant PSF (Ehrenfried and Koop, 2007) but are not relevant in the deep-sea context: the region of interest can be very large (easily greater than 10 000 m^2), with respect to the array dimension (a few meters). As an alternative, greedy methods such as CLEAN algorithms have been proposed for acoustic imaging, namely, because of their low computational cost, equivalent to only a few times the CBF running time (Merino-Martínez *et al.*, 2019; Sijtsma, 2007; Sijtsma *et al.*, 2017). They iteratively remove PSFs around maximum values found within CBF maps. In particular, CLEAN based on spatial source coherence (CLEAN-SC) is a promising approach, since it iteratively removes a "projected PSF," corresponding to the PSF fitted onto the data to further enhance the sidelobe rejection (Sijtsma, 2007).

The previously discussed aspects are investigated within a specific underwater acoustic application, deep-sea mining, presented in Fig. 1. A localization plane parallel and close to the seafloor is considered to capture the acoustic source of interest (e.g., the noisy industrial digging machine to be monitored). This localization plane is referred to as the *source plane*. The acoustic disturbing noise source is located on the *disturbing plane* (e.g., a passing boat). Therefore, a three-dimensional (3D) geometry problem has to be considered. Its good performance and low computation cost make the CLEAN-SC algorithm an interesting candidate for such 3D imaging problems (Sarradj, 2012b).

In this study, the authors propose an alternative to classical CBF for underwater acoustic imaging through four original contributions:

- Taking advantage of prior information on the *source plane* depth and the *disturbing plane* depth, it is demonstrated that it is sufficient and efficient to consider only these two reconstruction planes to perform multiplane imaging rather than using a dense 3D volume. Such multiplane imaging allows the disturbing sources to be located on the *disturbing plane* only (after deconvolution) and in this way de-noises the *source plane*. Also, this approach dramatically reduces the number of pixels and thus saves computation cost.
- The CLEAN-SC greedy deconvolution approach is introduced in the context of acoustic imaging in deep-sea environments. Interfering artifacts are removed from acoustic maps, and thus, simultaneous accurate estimations of position and source level are possible.
- CLEAN-SC is implemented in an unusual and challenging configuration for which the source is far from the array (with respect to the array length). Indeed, it has been reported that for DAMAS, the farther away the source is, the worse the deconvolution performance is (Brooks and Humphreys, 2005).
- This acoustic imaging strategy is illustrated and validated on experimental data acquired in a deep-sea mining environment with a controlled broadband source immersed at 700 m depth.

The paper is organized as follows. Section 2 contains four descriptions: the signal model, a classical two-step procedure based on CBF, the CLEAN-SC deconvolution, and finally the multiplane imaging approach. Methods are then compared using experimental data: the setup is presented (Sec. 3), and the results are analyzed (Sec. 4). A discussion and conclusions (Sec. 5) end the paper.

2. Methods

The goal of this application is to simultaneously locate the acoustic source and estimate its level. In this part, the signal model is introduced, and then the classic two-step procedure using CBF is presented with its limitations. To overcome the latter, the principle of acoustic map deconvolution is introduced, considering the CLEAN-SC approach (Sijtsma, 2007; Sijtsma *et al.*, 2017). Finally, the need for multiplane CLEAN-SC deconvolution in such configurations is explained.

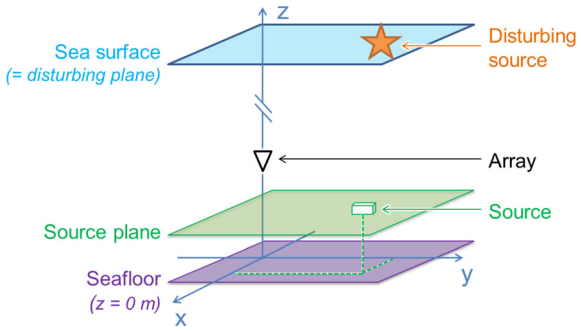

Fig. 1. Array configuration scheme with the *source plane* and *disturbing plane*.

2.1 Signal model

The data received on the array composed of M hydrophones, from a single source placed at $\vec{r}_0$, are modeled as an M-length vector at a given frequency f, as

$$\mathbf{p}(\vec{r}_0) = a_0 \frac{e^{-i2\pi f \mathbf{d}(\vec{r}_0)/c}}{\mathbf{d}(\vec{r}_0)} = a_0 \mathbf{g}(\vec{r}_0), \tag{1}$$

with a_0 the complex amplitude of the source, $\mathbf{d}(\vec{r}_0)$ the column-vector of length M containing the distances between the source and each hydrophone on the array, c the speed of sound, and $\mathbf{g}(\vec{r}_0)$ the free-field propagation vector. If several sources are considered, the basic principle of superposition is applied. Note that frequency dependence is omitted for the sake of clarity throughout this paper.

2.2 Conventional beamforming: Formulations and limits

CBF is a common and rather efficient approach to source localization. Each pixel value at position $\vec{r} = (x, y, z)$ (on the reconstructed imaging map) is denoted as $b(\vec{r})$ and is obtained applying the steering vector $\mathbf{h}(\vec{r})$ to the data as

$$b(\vec{r}) = \mathrm{E}\langle |\mathbf{h}^*(\vec{r})\mathbf{p}(\vec{r}_0)|^2 \rangle = \mathbf{h}^*(\vec{r})\,\mathbf{C}\,\mathbf{h}(\vec{r}), \tag{2}$$

with $\mathrm{E}\langle\cdot\rangle$ the expected value and the cross-spectral density matrix (CSM) defined as $\mathbf{C} = \mathrm{E}\langle \mathbf{p}(\vec{r}_0)\mathbf{p}^*(\vec{r}_0)\rangle$. Several formulations can be considered for the steering vector $\mathbf{h}(\vec{r})$. As shown in Sarradj (2012b), CBF cannot efficiently estimate both acoustic source position and level simultaneously. On the one hand, it is possible to accurately locate the source position while introducing a bias on power estimation and only compensating for phase shifts,

$$\mathbf{h}_{pos}(\vec{r}) = \frac{e^{-i2\pi f \mathbf{d}(\vec{r}_0)/c}}{M}. \tag{3}$$

On the other hand, an accurate power estimate can be achieved, but with a bias on position estimate, when further compensation for propagation attenuation is introduced,

$$\mathbf{h}_{lvl}(\vec{r}) = \mathbf{d}(\vec{r}_0)\frac{e^{-i2\pi f \mathbf{d}(\vec{r}_0)/c}}{M}. \tag{4}$$

Note that in Sarradj (2012b), the sources are very close to the array; relatively small biases are introduced regardless of the formulation used. However, in the present configuration, sources are relatively far from the array; the biases could be relatively large. For this reason, a two-step CBF should be used. First, the source is accurately located with CBF using $\mathbf{h}_{pos}(\vec{r})$, considering $\vec{r}_{\max}$ the location of the map's maximum value. Then the unbiased power (or source level) is estimated with CBF using $\mathbf{h}_{lvl}(\vec{r}_{\max})$ (where *lvl* stands for level).

CBF is classic and robust but faces two major limitations. First, the two-step process precludes considering the source distribution and its accurate power estimation at the same time. Furthermore, CBF produces maps on which each source is identified with a potentially wide PSF composed of one mainlobe centered on the actual source position and several sidelobes. The mainlobe's excessive extension, the strong sidelobes, and/or a powerful source's back lobe can partially or completely mask other weaker sources of interest (Cox and Lai, 2009).

2.3 Deconvolution of acoustic images with CLEAN-SC

Deconvolution approaches are powerful algorithms that aim to remove the effect of PSF spreading on acoustic imaging maps reconstructed with CBF (Ehrenfried and Koop, 2007; Leclère *et al.*, 2017; Merino-Martínez *et al.*, 2019; Sun *et al.*, 2020), providing enhanced source level estimation and weak source localization. The goal is to find an estimated $\mathbf{q}$ of the theoretic source distribution $\mathbf{q}_{th}$ spanning N grid points (often chosen as equal to the number of the beamformed pixels), with the grid points' respective transmitted powers [e.g., for single source scenario $\mathbf{q}_{th}(\vec{r}_0) = \sigma_0^2 = |a_0|^2$ and 0 elsewhere], that would produce the beamformed map $\mathbf{b}$, given by (2). Note that $\mathbf{q}$, $\mathbf{q}_{th}$, and $\mathbf{b}$ are N-length column-vectors that concatenate all image lines. $\mathbf{q}$ and $\mathbf{b}$ are often called the clean map and the dirty map, respectively.

CLEAN algorithms are greedy algorithms for deconvolution (Sijtsma, 2007; Sijtsma *et al.*, 2017), very efficient in terms of computational cost. They iteratively detect the maximum pixel value in the dirty map $\mathbf{b}$ and compute and remove the corresponding PSF at these locations to estimate $\mathbf{q}$. In particular, CLEAN-SC is widely used (e.g., in aeroacoustics), since it fits the modeled PSF to the data prior to removal from the map. Briefly, for each iteration, the theoretical steering vector is projected on an updated CSM; this projected steering vector is used to compute the projected PSF to be removed from the map, and its contribution is removed from the updated CSM.

The classic CLEAN-SC procedure is applied as described in Sijtsma (2007) and Sijtsma *et al.* (2017). As recommended by the conclusions of Sarradj (2012a), particular attention must be paid to the choice of the deconvolved dirty map to limit the biases on position and power level estimate, namely, because they could be exacerbated considering the following far-field scenario:

- For the initialization, ith iteration with $i = 0$, the dirty map $\mathbf{b}^{(0)}$ is chosen as $\mathbf{b}_{pos}$, i.e., the CBF map obtained with the steering vector formulation $\mathbf{h}_{pos}(\vec{r})$ in (3).
- Then, after the scheduled I_0 number of iterations (e.g., equal to the expected number of sources) of CLEAN-SC procedure, the obtained clean map $\mathbf{q}^{(I_0-1)}$ is accurate in terms of localization, as CBF with $\mathbf{h}_{pos}(\vec{r})$ has been considered, but it suffers from a strong bias in terms of power estimates. Thus, the final clean map $\mathbf{q}$ is obtained while compensating for the attenuation due to propagation, $\mathbf{q}(\vec{r}) = d_0^2(\vec{r})\,\mathbf{q}^{(I_0-1)}(\vec{r})$, with $d_0(\vec{r})$ the distance between the pixel position $(\vec{r})$ and the center of the array.

In this way, a sparse clean map $\mathbf{q}$ is obtained, with as many detected sources as I_0 (i.e., nonzero pixels). It provides an accurate localization and also an unbiased source level with the compensation for propagation attenuation. A simple implementation of the CLEAN-SC is performed, but a stop criterion based on the norm of $\mathbf{C}^{(i)}$ (the CSM at the iteration i) can be further introduced when the number of sources is unknown, as well as a loop gain to tune the convergence of the algorithm (Sijtsma, 2007).

2.4 Two-dimensional (2D), 3D, or multiplane imaging

A scheme of the configuration is given in Fig. 1 (with the z axis pointing upward). In practical applications, the source of interest has to be located in a given plane, the *source plane*, parallel to the seafloor ($z = 0$ m). However, when such sources transmit low-power noise, disturbing sources on the sea surface's (*disturbing plane*) (even far away, hundreds of meters) are no longer negligible and will interfere with the source. Consequently, such disturbing acoustic sources have to be taken into account in the imaging process; the issue becomes a 3D problem.

CBF is a pixelwise procedure: each pixel value on the grid is completely independent of the other pixel values and also does not depend on the chosen reconstruction grid. Considering a 2D grid, or rather extracting the corresponding plane from a full 3D image, will lead to the same image (whether the source distribution is 2D or 3D).

However, this is absolutely not the case for deconvolution. Indeed, such approaches aim to find the source distribution $\mathbf{q}_{th}$, lying in the chosen reconstruction grid that best ("best" depending on the chosen algorithm) explains the reconstructed dirty map (i.e., 2D or 3D image obtained with CBF) (Ehrenfried and Koop, 2007). CLEAN-SC has already been used to efficiently address 3D imaging problems for which the sources are close compared to the array dimension (Sarradj, 2012b). In the context of underwater acoustics, the imaging problem's dimensions could be significantly greater: the ratio between the array size and the relative distances to sources could be on the order of 10 or 100. Therefore, a dense 3D reconstruction grid (i.e., with a dense plane distribution along the z plane) would not be efficient in terms of computation.

To introduce more information as input to the CLEAN-SC algorithm, while keeping a relatively small numbers of pixels, prior knowledge of the problem's geometry is exploited; only the *source plane* and the *disturbing plane* are considered for the reconstruction process. This approach is referred to as "multiplane imaging."

3. Deep-sea mining experimental setup

The experiment took place in deep water to mimic a deep-sea mining configuration with excavation machines. The disturbing source was a boat on the surface. The relative positions for the boat, the array, and the transmitting source were accurately estimated with an auxiliary active acoustic system as ground truth. The seafloor was 700 m below the surface. To mimic excavation machines, a controlled source transmitting broadband noise was placed close to the seafloor (not on it for practical purposes). The corresponding spectrum represents typical noise produced by machines scraping the seafloor. It is composed of a constant level (plateau) between 1 and 3 kHz, followed by a 20 dB/decade decrease. The transmitted noise lasts for 30 s, with a varying transmission power for the plateau from 75 to 120 dB re 1 μPa at 1 m. A 3 m conical array composed of 21 microphones (Baron *et al.*, 2021) was placed 40 m above the seafloor. The acoustic signals were acquired with a sampling frequency of 25 kHz for 30 s. In this studied experimental configuration, the source was located at the depth $z = 18$ m (*source plane*). When this source transmitted very low-power noise, the boat noise on the surface at $z = 700$ m (*disturbing plane*) was no longer negligible and interfered with the source. Consequently, it had to be taken into account in the imaging process; the multiplane imaging process was used. The speed of sound is supposed to be constant as the configuration is vertical, so undesired effect due to inhomogeneous speed of sound, such as horizontal refraction, can be neglected (Munk *et al.*, 2009). Moreover, the method is derived considering the direct acoustic paths prevail, so, for this configuration, the potential reflections from the seabed are neglected. The assumption could be reconsidered in the presence of a highly reflecting seabed.

4. Results

Maps are displayed in Figs. 2 and 3. The reconstruction frequency is $f = 2300$ Hz, and the CSM is estimated using 90 ms snapshot averaging with Hann windowing, no overlap, on the full acquisition duration of 30 s. The speed of sound for reconstruction is assumed to be constant in the all-water column and equal to 1517 m/s. The ground truth positions of the source and the boat, indicated in Figs. 2 and 3, are the centers of uncertainty regions described by circles of radius 7 m for the source and 5 m for the boat.

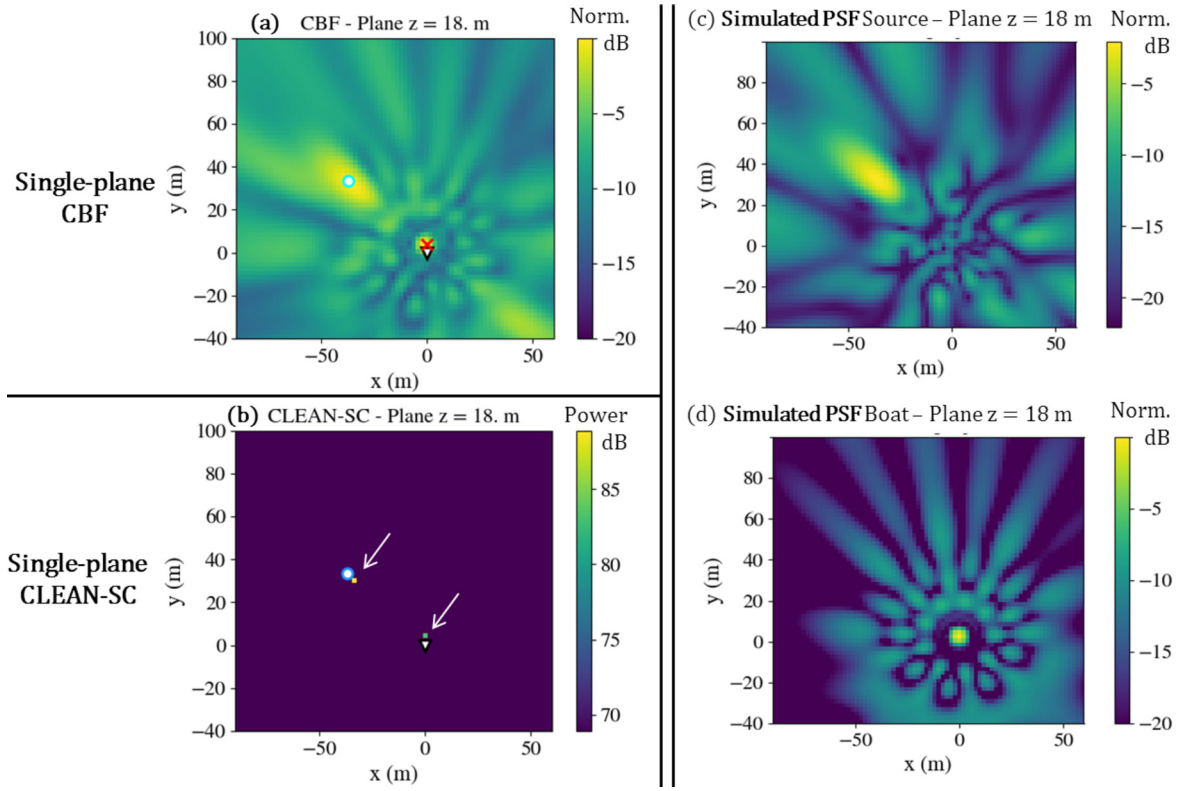

Fig. 2. Acoustic source mapping of a broadband source transmitting at 90 dB re 1 μPa at 1 m, within the band 1–3 kHz, placed at (–36, 32, 18) m [blue circle in (a) and (b)]. The boat is 700 m above the seafloor. The array is centered at (0, 0, 40) m; see Fig. 1 [its projection on the maps is represented by a black/white triangle in (a) and (b)]. Maps are reconstructed at $f = 2300$ Hz, considering only the *source plane* at $z = 18$ m. (a) CBF with h_{pos} is normalized and (b) CLEAN-SC is not normalized. The red cross in (a) represents the maximum map value. The white arrows in (b) indicate the nonzero pixel values on CLEAN-SC. The simulated contributions in the *source plane* for sources located at the ground truth locations of the (c) source and (d) boat are normalized and displayed.

4.1 CBF limitations

Figure 2(a) shows the 2D map obtained using CBF (with $\mathbf{h}_{pos}$) from the acoustic signals received while the source transmitted at 90 dB re 1 μPa at 1 m, within the band 1–3 kHz (i.e., within the plateau). Two strong local maxima are observed: the global maximum close to $(x = 0, y = 0)$ (red cross) and a second one located close to the transmitting source's position (blue circle) within the uncertainty region of 7 m. This map [Fig. 2(a)], obtained from experimental data, corresponds well to the superposition of the two simulated contributions: the source of interest [Fig. 2(c)] and the boat [Fig. 2(d)] on the *source plane*. These simulations were done using the available source and boat ground truth locations. Two observations can be made: first, the most intense spot originates from the boat noise (referred to as the boat artifact in the following comments), and second, the source localization is limited due to the boat sidelobes (the latter can even completely mask the source mainlobe on maps in other configurations for which the source power is lower, not shown here). Note that the centered and intense spot in Fig. 2(d) results from the back lobe [i.e., reconstruction artifact that appears as a ghost source, rather symmetric to the source with respect to the array (Cox and Lai, 2009)], while the other diffused stains are sidelobes.

4.2 Shortcomings of CLEAN-SC using only the source plane

The map obtained for CLEAN-SC considering only the CBF map of the *source plane* [Fig. 2(a)] is shown in Fig. 2(b). This map only contains two nonzero values: 83 dB for the first detected maximum value from the boat artifact in Fig. 2(a) (red cross) and 89 dB for the second one corresponding to the transmitting source. Note that the source level estimate ranking is changed due to the compensation with $d_0^2(\vec{r})$: the first detected maximum [red cross in Fig. 2(a)] has been erroneously interpreted by CLEAN-SC as resulting from a source located in the *source plane*. A first consequence is that potentially, the removed projected PSF does not rigorously fit the whole artifacts that originated from the boat on the sea surface, with a risk of biasing the following iterations. A second consequence impacts the CLEAN-SC map [Fig. 2(b)], which contains a nonphysical boat artifact that is misinterpreted as a fake second source at $z = 18$ m.

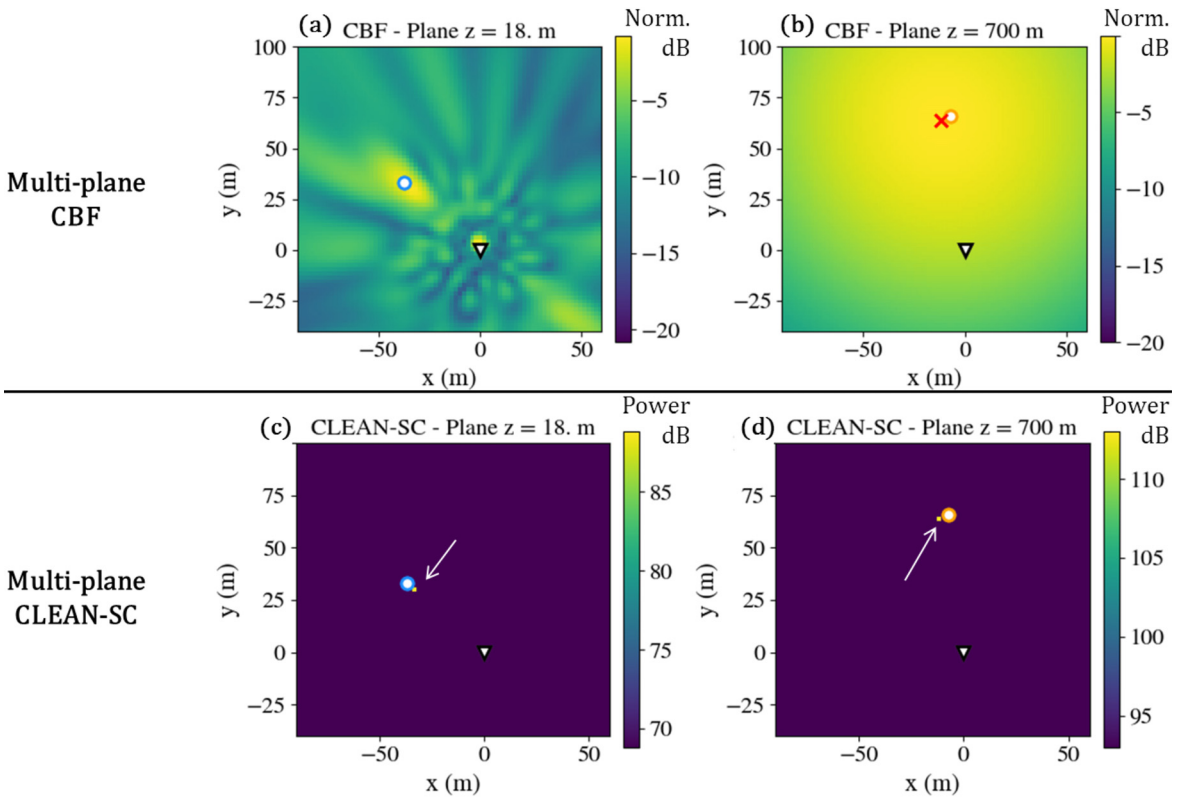

Fig. 3. Acoustic source mapping of a broadband source transmitting at 90 dB re 1 μPa at 1 m, within the band 1–3 kHz, located at (–36, 32, 18) m [blue/white circle in (a) and (c)]. The boat was located at (–7, 65, 700) m [orange/white circle in (b) and (d)]. The array was centered at (0, 0, 40) m [black/white triangle is its projection on the plane in (a) and (c)]. Maps are reconstructed at $f = 2300$ Hz, considering two planes: the *source plane* at $z = 18$ m [(a), (c)] and the *disturbing plane* at $z = 700$ m [(b), (d)]. CBF values with h_{pos} are normalized and presented in (a) and (b). The red cross in (b) represents the maximum CBF value on the two planes [(a), (b)]. Maps [(c), (d)] resulting from multiplane CLEAN-SC are not normalized, with arrows highlighting the nonzero pixel values.

4.3 CBF and CLEAN-SC using multiplane imaging

In Fig. 3, the two maps obtained with multiplane CBF (with $\mathbf{h}_{pos}$) are displayed for two reconstruction depths: $z = 18$ m corresponding to the *source plane* in Fig. 3(a) and $z = 700$ m corresponding to the sea surface in Fig. 3(b). On the latter, the mainlobe is centered around the actual boat position (orange circle), at the edge of the uncertainty region of 5 m. The maximum value on both CBF planes is located at the center of the *disturbing plane*'s mainlobe [red cross in Fig. 3(b)]. CLEAN-SC deconvolution is then applied to the two maps. The source corresponding to the CBF global maximum is recovered on the *disturbing plane* [Fig. 3(d)]. In this case, the removed projected PSF better fits the actual one, originating from the boat source. After one iteration, the second maximum value, corresponding to the source of interest, is detected within the uncertainty region of 7 m and recovered on the *source plane* by CLEAN-SC [Fig. 3(c)], with a power estimate of 89 dB (close to the theoretical 90 dB). Using multiplane CLEAN-SC [Fig. 3(c)], only the actual source is localized on the *source plane* (without any boat artifact) and with an accurate power estimate.

5. Discussion and conclusions

The CLEAN-SC deconvolution algorithm has been validated using experimental data in the context of underwater acoustic imaging. In particular, results demonstrate that using an additional *disturbing plane* makes it possible to de-noise the *source plane* of interest, not only compared to CBF, but also compared to CLEAN-SC when only the *source plane* is considered. The resulting maps are clean and can be easily interpreted, since they simultaneously provide both accurate localization and source level estimates. The computation time is kept close to that of CBF, as it is proportional to the number of planes (two in the present case) and to the number of iterations, corresponding here to the number of expected sources, i.e., two: thus, in this study the running time for CLEAN-SC multiplane procedure is about 4 times the two-step CBF approach. Finally, this approach is quite easy to handle, since its tuning is based on very concrete and physical parameters: the *disturbing plane* depth and the number of expected sources.

This work highlights the CBF limitations for accurate and simultaneous position and source level estimation (Sarradj, 2012b), which are amplified in the considered configuration (small array dimension compared to source distance).

Multiplane CLEAN-SC successfully de-noises the *source plane* of interest if the *disturbing plane* contains the maximum disturbing PSF value. It is empirically observed that the approach remains effective as long as the *disturbing plane* maximum belongs to the mainlobe of the disturbing PSF and is greater than the contribution of the disturbing source on the *source plane*. Consequently, the method is robust to uncertainties on the depth for the *disturbing plane*. Errors on the relative distance between the array and the sea surface, on the order of several tens of meters, are tolerated by the de-noising procedure, since the PSF slowly varies with respect to depth.

Future work will investigate the advantages and the limits of such robustness regarding *disturbing plane* position and dimension. This is expected to provide a systematic procedure to de-noise acoustic maps using deconvolution algorithms.

ACKNOWLEDGMENTS

This study was carried out within the framework of the FUI 22 collaborative project "Abysound," funded by Pôle Mer Méditerrannée and Banque Publique d'Investissement (BPI). The authors would like to thank all Abysound project partners: Naval Group, OSEAN SAS, MicrodB, Semantic TS, l'Institut Français de Recherche pour l'Exploitation de la Mer (IFREMER), Gipsa-Lab, the Laboratoire de Mécanique et d'Acoustique (LMA), and the Laboratoire des Sciences de l'Information et des Systèmes (LSIS). This work was performed within the framework of the LABEX CeLyA (ANR-10-LABX-0060) of Université de Lyon, within the program Investissements d'Avenir (ANR-16-IDEX-0005) operated by the French National Research Agency (ANR).

References and links

Baron, V., Finez, A., Bouley, S., Fayet, F., Mars, J. I., and Nicolas, B. (**2021**). "Hydrophone array optimization, conception, and validation for localization of acoustic sources in deep-sea mining," IEEE J. Ocean. Eng. **46**, 555–563.

Brooks, T., and Humphreys, W. (**2005**). "Three-dimensional applications of DAMAS methodology for aeroacoustic noise source definition," in *Proceedings of the 11th AIAA/CEAS Aeroacoustics Conference*, May 23–25, Monterey, CA, p. 2960.

Brooks, T. F., and Humphreys, W. M. (**2006**). "A deconvolution approach for the mapping of acoustic sources (DAMAS) determined from phased microphone arrays," J. Sound Vib. **294**(4), 856–879.

Capon, J. (**1969**). "High-resolution frequency-wavenumber spectrum analysis," Proc. IEEE **57**(8), 1408–1418.

Clark, C. W., Ellison, W. T., Southall, B. L., Hatch, L., Van Parijs, S. M., Frankel, A., and Ponirakis, D. (**2009**). "Acoustic masking in marine ecosystems: Intuitions, analysis, and implication," Mar. Ecol. Prog. Ser. **395**, 201–222.

Cox, H., and Lai, H. (**2009**). "Simultaneous grating lobe and backlobe rejection with a line array of vector sensors," in *2009 Conference Record of the Forty-Third Asilomar Conference on Signals, Systems and Computers*, November 1–4, Pacific Grove, CA, pp. 1320–1323.

Ehrenfried, K., and Koop, L. (**2007**). "Comparison of iterative deconvolution algorithms for the mapping of acoustic sources," AIAA J. **45**(7), 1584–1595.

Kuperman, W. A., and Roux, P. (**2007**). "Underwater acoustics," in *Springer Handbook of Acoustics* (Springer-Verlag, New York), pp. 149–204.

Leclère, Q., Pereira, A., Bailly, C., Antoni, J., and Picard, C. (**2017**). "A unified formalism for acoustic imaging based on microphone array measurements," Int. J. Aeroacoust. **16**(4), 431–456.

Li, J., White, P. R., Bull, J. M., and Leighton, T. G. (**2019**). "A noise impact assessment model for passive acoustic measurements of seabed gas fluxes," Ocean Eng. **183**, 294–304.

Merino-Martínez, R., Sijtsma, P., Snellen, M., Ahlefeldt, T., Bahr, C., Blacodon, D., Ernst, D., Finez, A., Funke, S., Geyer, T., Haxter, S., Herold, G., Huang, X., Humphreys, W., Leclère, Q., Malgoezar, A., Michel, U., Padois, T., and Spehr, C. (**2019**). "A review of acoustic imaging methods using phased microphone arrays," CEAS Aeronaut. J. **10**, 197–230.

Munk, W., Worcester, P., and Wunsch, C. (**2009**). *Ocean Acoustic Tomography* (Cambridge University Press, Cambridge, UK).

Pham, G.-T., Baron, V., Finez, A., Mars, J. I., and Nicolas, B. (**2019**). "High resolution source localization in underwater acoustics for deep sea mining monitoring," in *Proceedings of OCEANS 2019-Marseille*, June 17–20, Marseille, France, pp. 1–7.

Sarradj, E. (**2012a**). "Three-dimensional acoustic source mapping," in *Proceedings on CD of the 4th Berlin Beamforming Conference*, February 22–23, Berlin, Germany.

Sarradj, E. (**2012b**). "Three-dimensional acoustic source mapping with different beamforming steering vector formulations," Adv. Acoust. Vib. **2012**, 292695.

Sijtsma, P. (**2007**). "Clean based on spatial source coherence," Int. J. Aeroacoust. **6**(4), 357–374.

Sijtsma, P., Merino-Martinez, R., Malgoezar, A., and Snellen, M. (**2017**). "High-resolution CLEAN-SC: Theory and experimental validation," Int. J. Aeroacoust. **16**(4), 274–298.

Stoica, P., Wang, Z., and Li, J. (**2003**). "Robust Capon beamforming," IEEE Signal Process. Lett. **10**(6), 172–175.

Sun, D., Ma, C., Mei, J., and Shi, W. (**2020**). "Improving the resolution of underwater acoustic image measurement by deconvolution," Appl. Acoust. **165**, 107292.